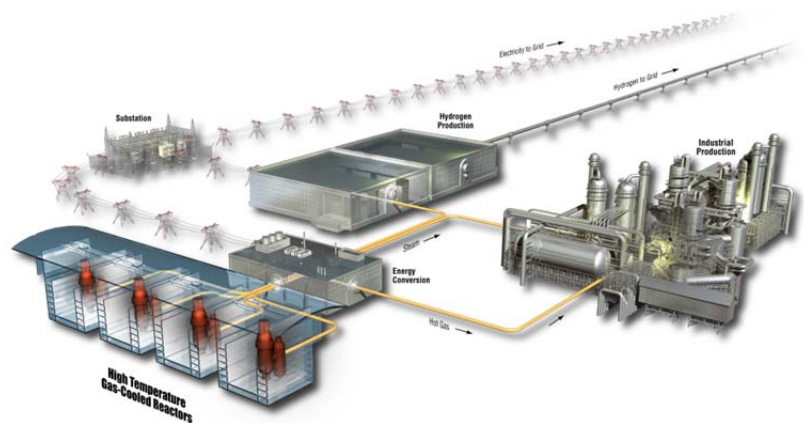


High Temperature Gas-Cooled Test Reactor Options Status Report

James W. Sterbentz
Paul D. Bayless

August 2015

The INL is a
U.S. Department of Energy
National Laboratory
operated by
Battelle Energy Alliance



DISCLAIMER

This information was prepared as an account of work sponsored by an agency of the U.S. Government. Neither the U.S. Government nor any agency thereof, nor any of their employees, makes any warranty, expressed or implied, or assumes any legal liability or responsibility for the accuracy, completeness, or usefulness, of any information, apparatus, product, or process disclosed, or represents that its use would not infringe privately owned rights. References herein to any specific commercial product, process, or service by trade name, trade mark, manufacturer, or otherwise, does not necessarily constitute or imply its endorsement, recommendation, or favoring by the U.S. Government or any agency thereof. The views and opinions of authors expressed herein do not necessarily state or reflect those of the U.S. Government or any agency thereof.

High Temperature Gas-Cooled Test Reactor Options Status Report

James W. Sterbentz
Paul D. Bayless

August 2015

Idaho National Laboratory
INL ART TDO Program
Idaho Falls, Idaho 83415

<http://www.inl.gov>

Prepared for the
U.S. Department of Energy
Office of Nuclear Energy
Under DOE Idaho Operations Office
Contract DE-AC07-05ID14517

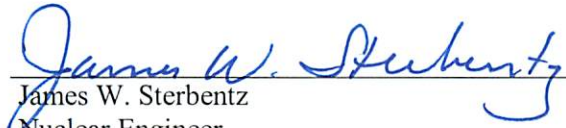
INL ART TDO Program

High Temperature Gas-Cooled Test Reactor Options
Status Report

INL/EXT-15-36340

August 2015

Authors:

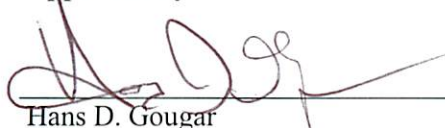

James W. Sterbentz
Nuclear Engineer

8-28-2015
Date


Paul D. Bayless
Nuclear Engineer

8/28/2015
Date

Approved by:


Hans D. Gougar
INL ART TDO Deputy Technical Director

8/28/2015
Date


Daren K. Jensen
INL ART TDO Quality Assurance

8/27/2015
Date

ABSTRACT

Preliminary scoping calculations are being performed for a 100 MW gas-cooled test reactor. The initial design uses standard prismatic blocks and 15.5% enriched UCO fuel. Reactor physics and thermal-hydraulics simulations have been performed to identify some reactor design features to investigate further. Current status of the effort is described.

CONTENTS

| | |
|--|-----|
| ABSTRACT..... | vii |
| 1. Introduction..... | 1 |
| 2. Reactor Physics..... | 3 |
| 2.1 Physics Model..... | 3 |
| 2.2 Physics Parameter Limitations..... | 3 |
| 2.3 Criticality..... | 5 |
| 2.4 Irradiation Total Flux..... | 8 |
| 2.5 Power-Peaking..... | 11 |
| 2.6 Average Particle Power..... | 11 |
| 3. Thermal Hydraulics..... | 13 |
| 3.1 Input Model Description..... | 13 |
| 3.2 Steady State Simulations..... | 14 |
| 3.2.1 Scoping Sensitivity Studies..... | 15 |
| 3.2.2 Steady State..... | 16 |
| 3.2.3 Sensitivity Analyses..... | 16 |
| 3.3 Transient Simulations..... | 18 |
| 4. Summary and Future Work..... | 24 |
| 5. References..... | 26 |

FIGURES

| | |
|---|----|
| Figure 1-1. Reactor vessel cross section in the core region..... | 1 |
| Figure 2-1. Cross-sectional view of the 18-column core (baseline core)..... | 4 |
| Figure 2-2. Cross-sectional view of the 6-column core..... | 4 |
| Figure 2-3. Cross-sectional view of the 12-column core..... | 5 |
| Figure 2-4. K-effective versus PF for the three core configurations..... | 6 |
| Figure 2-5. K-effective versus the total U-235 core mass loading for the three core configurations..... | 7 |
| Figure 2-6. K-effective versus packing fraction and fuel rod radius for the 18-column core..... | 8 |
| Figure 3-1. Nodalization of the reactor vessel for the gas test reactor RELAP5-3D input model..... | 14 |
| Figure 3-2. Peak fuel temperatures for the DCC transients..... | 19 |
| Figure 3-3. Axial temperature distribution in the inner fuel ring graphite for DCC transient Case 1..... | 19 |
| Figure 3-4. Average fuel temperatures for the DCC transients..... | 20 |
| Figure 3-5. Temperatures in the central reflector and fuel ring graphite for the DCC transients..... | 20 |
| Figure 3-6. Temperatures in the outer reflector for the DCC transients..... | 21 |

| | |
|---|----|
| Figure 3-7. Temperatures in the PSR, core barrel, and reactor vessel for the DCC transients. | 21 |
| Figure 3-8. Core heat generation and RCCS heat removal for the DCC transients. | 22 |
| Figure 3-9. RCCS coolant outlet temperature for the DCC transients. | 22 |
| Figure 3-10. Reactor cavity gas temperature for the DCC transients. | 23 |

TABLES

| | |
|---|----|
| Table 2-1. Maximum total flux for the 6-column core at select locations in the core. | 9 |
| Table 2-2. Maximum total flux for the 12-column core at select locations in the core. | 9 |
| Table 2-3. Maximum total flux for the 18-column core (baseline) at select locations in the core. | 9 |
| Table 2-4. Fuel rod maximum peak-to-average power. | 11 |
| Table 2-5. Average TRISO fuel particle power estimates in the 6-column core. | 11 |
| Table 2-6. Average TRISO fuel particle power estimates in the 12-column core. | 12 |
| Table 2-7. Average TRISO fuel particle power estimates in the 18-column core. | 12 |
| Table 3-1. Inner core ring fuel rod average temperatures from the fuel rod diameter sensitivity calculations. | 15 |
| Table 3-2. Center irradiation hole size sensitivity calculation results. | 15 |
| Table 3-3. Sensitivity on gap size around water-filled center irradiation tube. | 16 |
| Table 3-4. Steady state conditions. | 16 |
| Table 3-5. Block-to-block gap width sensitivity study results. | 17 |
| Table 3-6. Effect of crossflow on gap outlet temperatures (°C). | 18 |

High Temperature Gas-Cooled Test Reactor Options Status Report

1. Introduction

A point design for a high temperature gas-cooled test reactor is being developed. The design accommodates independently-cooled irradiation positions (loops) in the central and outer reflectors that can contain different working fluids, such as high-pressure water or molten salt. The graphite reflector can also accommodate a large number of non-loop irradiation holes for “drop-in” capsule experiments cooled by helium. Preliminary scoping calculations are being performed to provide insight toward a design to be investigated further; results of the analyses performed thus far are presented.

The design uses standard gas-reactor components. The fuel is 15.5% enriched UCO. The fuel blocks are the typical General Atomics design (DOE/HTGR-86-024, 1986), containing 210 fuel rods and 108 coolant holes in a 0.793-m high, 0.360-m wide hexagonal graphite block. Control rods are located in the outer reflector. Figure 1-1 shows a cross section of the reactor vessel and core for the current baseline 18-column core configuration that is being analyzed.

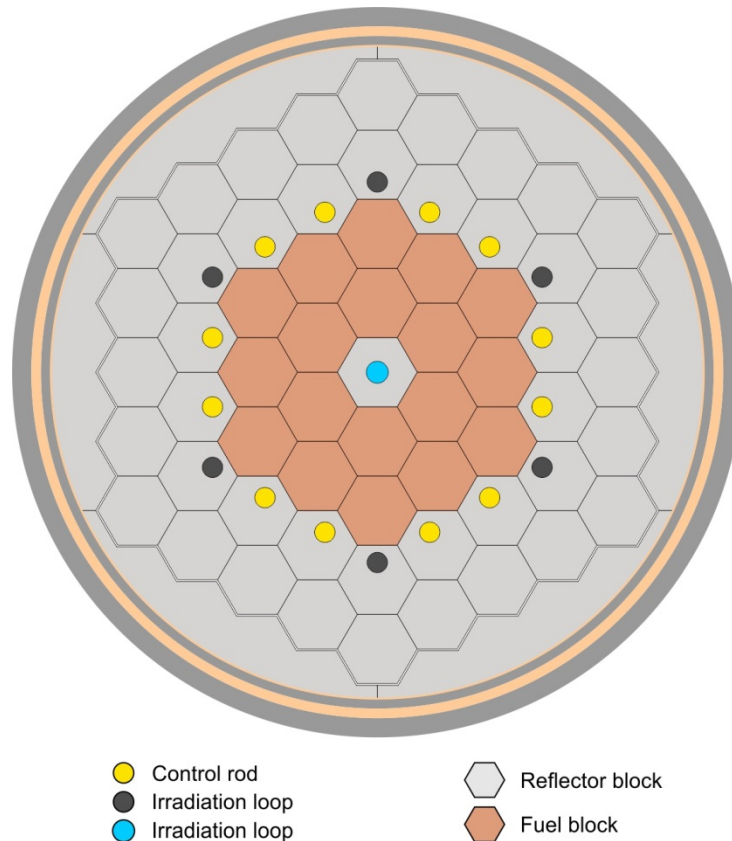


Figure 1-1. Reactor vessel cross section in the core region.

This 18-column baseline configuration is modeled with coolant flow entering near the bottom of the reactor vessel cylinder, flowing up through the annulus between the core barrel and reactor vessel, then entering the upper plenum. Helium then flows down through a number of parallel channels in the core: the coolant holes in the fuel blocks, the gaps between the hexagonal blocks, the gap between the permanent side reflector (PSR) and the core barrel, and gaps between the graphite reflector blocks and the

control rods or irradiation tubes. These flow paths all meet in the lower plenum, from which the coolant exits the reactor vessel.

The core consists of a central graphite reflector block with an irradiation loop facility located in the center. Moving radially, the next two rings contain fuel blocks. The first ring of the side reflector contains holes for 12 control rods and 6 irradiation tubes. There is a second ring of side reflector blocks, then the PSR and core barrel. The nominal core power is 100 MW. The core is eight blocks high, with top and bottom reflectors of 1.189 and 1.585 m, respectively.

A simple model of a cavity cooling system has also been developed to allow scoping accident calculations to be performed. Water at 27°C flows through cooling panels completely surrounding the reactor vessel, driven by natural circulation from a large overhead tank from which heat can be rejected to the atmosphere.

The initial efforts have focused on the core design. Details of the reactor physics and thermal hydraulics investigations are provided in the sections that follow.

2. Reactor Physics

2.1 Physics Model

Preliminary physics scoping calculations have been performed using the MCNP computer code (X-5 Monte Carlo Team, 2003) on the Idaho National Laboratory supercomputer systems. The 18-column core configuration (Figure 1-1) was conceived simply as a basis or starting point from which to begin the physics and thermal-hydraulic parametric evaluations. The 18-column core configuration resembles the larger-in-size and higher-in-power annular high temperature gas-cooled reactor (HTGR) designs previously developed, but the number of fuel columns for the smaller HTGR test reactor has been substantially reduced reflecting the lower 100 MW total core power goal. Figure 2-1 shows the 18-column core and is the same as Figure 1-1 for easy comparison to the two additional core configurations that follow.

The 18-column core model is the current baseline model. Each of the 18 fuel columns consists of a stack of eight hexagonal fuel blocks with a top and bottom graphite block acting as a reflector. Each fuel block in the stack is assigned a level number. For example, the fuel blocks at the bottom of each stack are referred to as Level 1 and the fuel blocks at the top of the stack are Level 8. The core is annular with both an inner and outer graphite reflector, although the inner reflector is just a single graphite block column with a central irradiation facility or hole. The six outer irradiation holes are located in the first ring of the outer reflector along with empty control rod holes.

An MCNP model of this 18-column core has been constructed, plotted, and executed as part of the initial physics scoping assessment. The fully three-dimensional core model consists of eight axial fuel block levels plus a top and bottom level for the graphite end reflector blocks. The core has six radial rings of blocks for a total of 910 block locations, of which 144 are fuel blocks (8 levels \times 18 columns). Each fuel block has 210 fuel rods, 110 coolant channels, and six burnable poison rod channels currently filled with graphite. To reduce the size of the MCNP core model so it would run more efficiently for parametric analyses, a one-twelfth (1/12) core model was constructed with reflective boundary conditions applied to the radial sides of the three-dimensional wedge, thereby creating a neutronically full-core equivalent representation. All core models herein use fresh fuel, with no depletion yet. All calculated data are for beginning-of-life and un-rodded conditions, as control rods have not been designed.

The thermal-hydraulic analysis provided block-average temperatures for the graphite and average fuel rod temperatures by block or ring and level. These temperatures were coupled into the physics models by using the corresponding temperature-dependent Doppler-broadened neutron cross section library data for the fission products and actinide nuclides and temperature-dependent thermal neutron scattering data or $S(\alpha,\beta)$ data for the bulk and compact matrix graphite.

In addition to the baseline 18-column core configuration, 6-column and 12-column core configurations are also part of the physics scoping calculations. MCNP models were constructed for these two additional cores with comparable parametric analyses performed for comparison to the 18-column core. Figures 2-2 and 2-3 show cross-sectional views of the 6-column and 12-column core configurations, respectively.

2.2 Physics Parameter Limitations

For the initial physics analysis, several parameters were held constant:

- (1) Uranium enrichment = 15.5 wt% U-235
- (2) TRISO particle kernel diameter = 425 μm
- (3) TRISO particle UCO density = 11.04 g/cm^3
- (4) TRISO particle coating thicknesses and particle diameter
- (5) Compact graphite matrix binder density = 1.70 g/cm^3

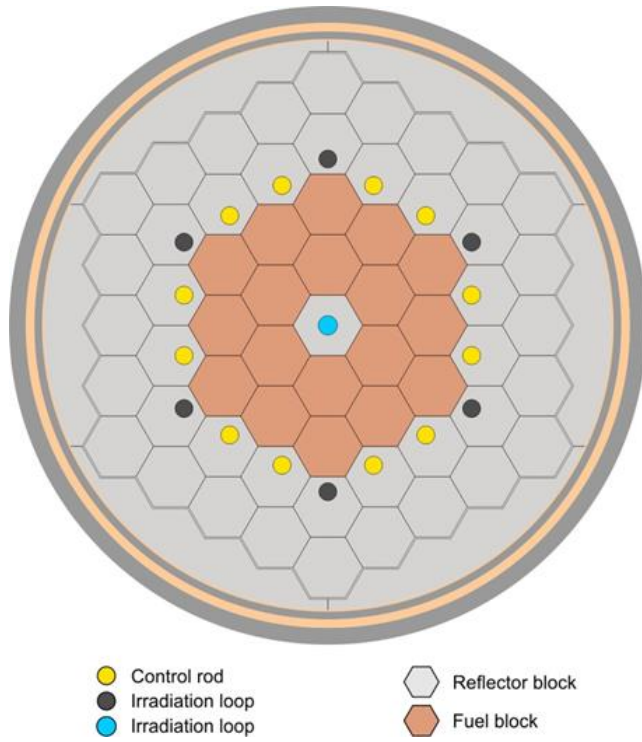


Figure 2-1. Cross-sectional view of the 18-column core (baseline core).

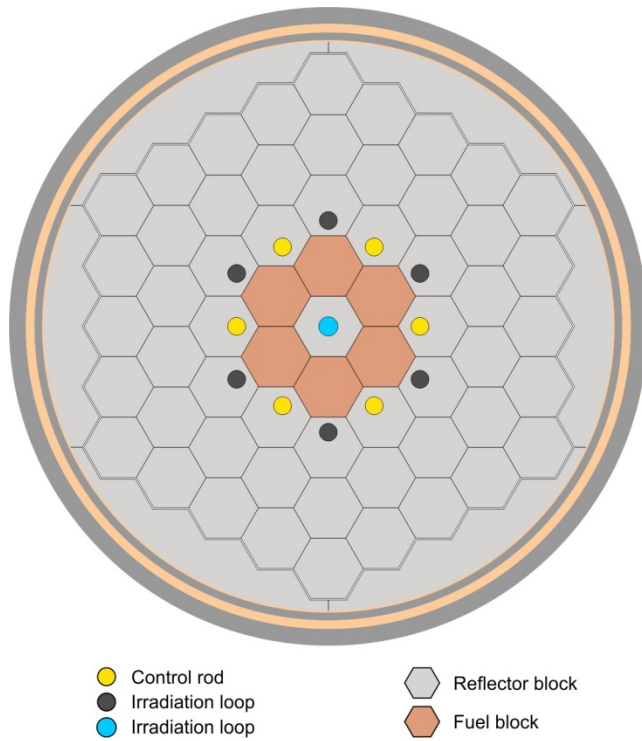


Figure 2-2. Cross-sectional view of the 6-column core.

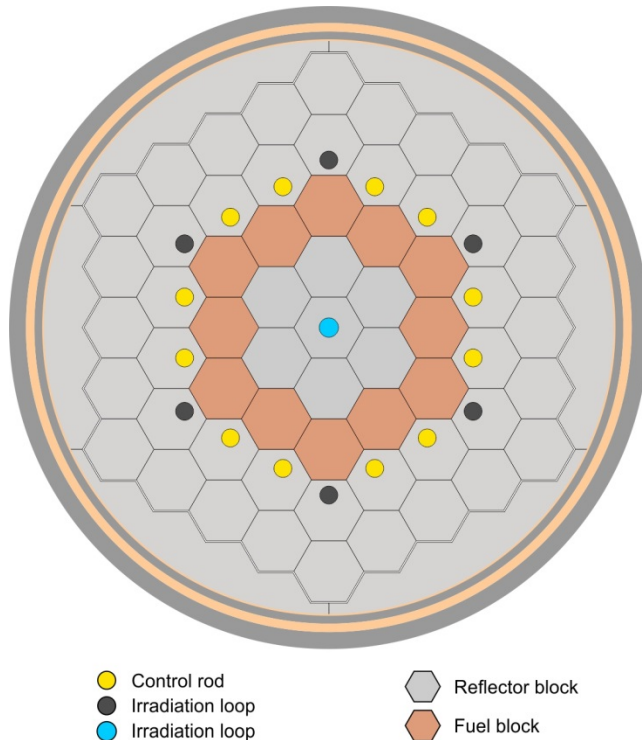


Figure 2-3. Cross-sectional view of the 12-column core.

- (6) Block graphite density = 1.83 g/cm³
- (7) Fuel rod radius (compact radius) = 0.6225 cm
- (8) Fuel and graphite blocks gross dimensions: flat-to-flat = 35.997 cm, height = 79.2987 cm, or basically the old Fort Saint Vrain (FSV) fuel block dimensions
- (9) Total core power = 100 MW.

The particle packing fraction (PF) in the fuel compacts was not fixed and was varied in all the parametric studies. Particle PF has a large impact on the compact and fuel block uranium mass loadings and therefore the fuel cycle length. Cycle length will be determined in future depletion studies. The fuel rod radius was varied in one scoping study. Core power level may increase later to boost irradiation fluxes. Many of these parameters can be varied in subsequent sensitivity and optimization studies.

2.3 Criticality

The first parametric study focused on core criticality. The two variables considered were the number of fuel columns and the particle packing fraction. The number of fuel columns is currently limited to the 6, 12, and 18-column models or 48, 96, and 144 fuel blocks, respectively. The 10 specific particle packing fractions considered were: PF=0.05, 0.10, 0.15, 0.20, 0.25, 0.30, 0.35, 0.40, 0.45, and 0.50.

Figure 2-4 is a plot of the core k-effective versus particle packing fraction for the three core configurations. The particle packing fraction is assumed to be uniform in each block and therefore the entire active core. Although all three cores are critical for PF>10%, it is not clear yet what minimum PF will achieve a desired cycle length and irradiation flux levels.

Depletion studies will be performed later to determine the cycle length for the three core configurations versus PF. If the PF variable on the x-axis in Figure 2-4 is replaced with a directly

proportional variable, namely, the total U-235 core mass loading, a crude estimate of the minimum PF can be determined for a desired cycle length at 100 MW. Figure 2-5 is a plot of the core k-effective versus total U-235 mass loading in the core. The 10 points on each curve in Figure 2-5 correspond directly to the 10 PF points on matching curves in Figure 2-4.

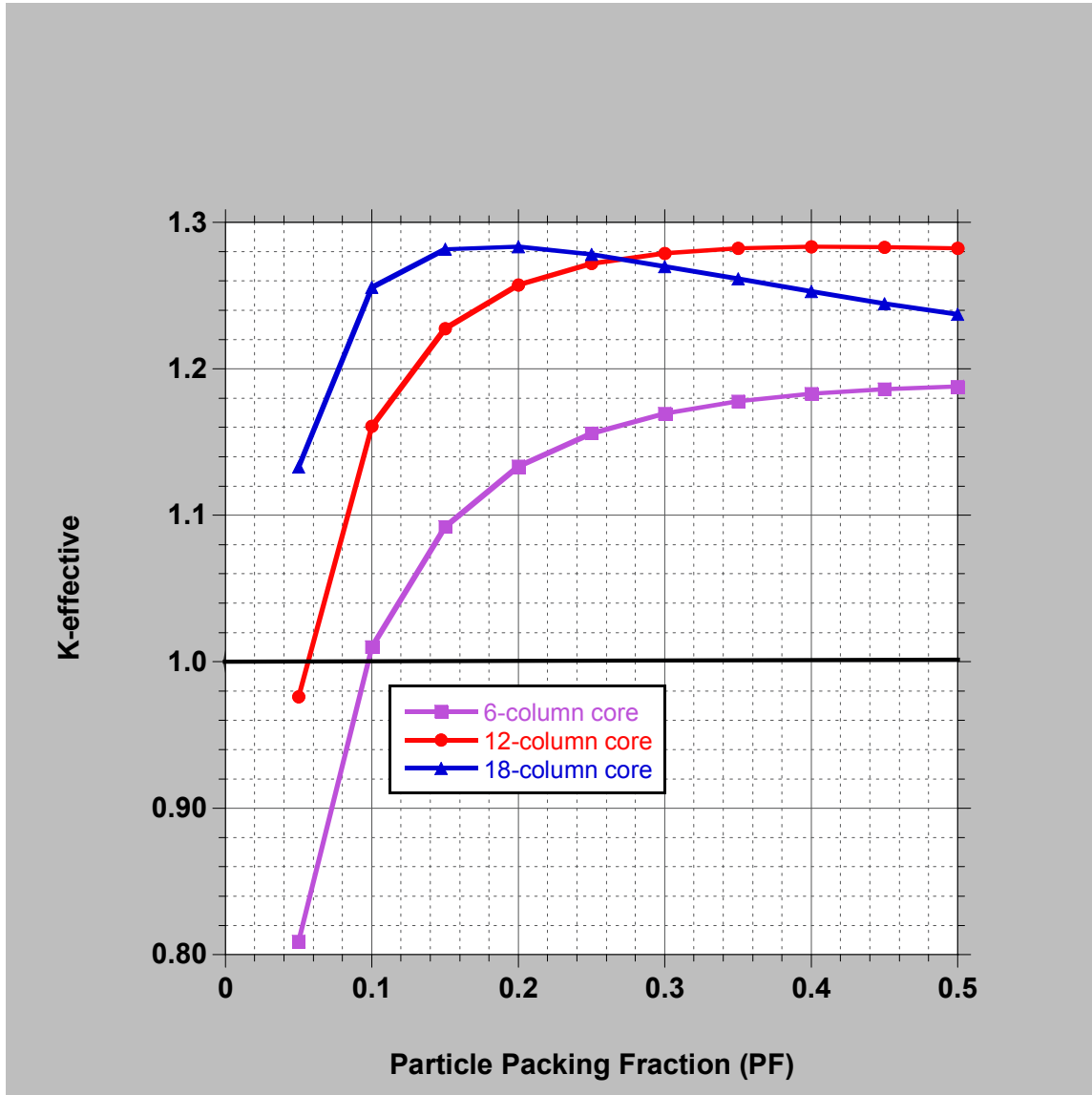


Figure 2-4. K-effective versus PF for the three core configurations.

If the total core power is assumed to be 100 MW and the desired cycle length is assumed to be one year (365 days), approximately 100 grams U-235 per day will be depleted, or 36.5 kg over the 1-year cycle. Therefore, roughly a minimum of 50 kg U-235 in an initial core load will be required to maintain criticality over the cycle. This translates into minimum packing fractions:

- 6-column core: PF>30%
- 12-column core: PF>15%
- 18-column core: PF>10%.

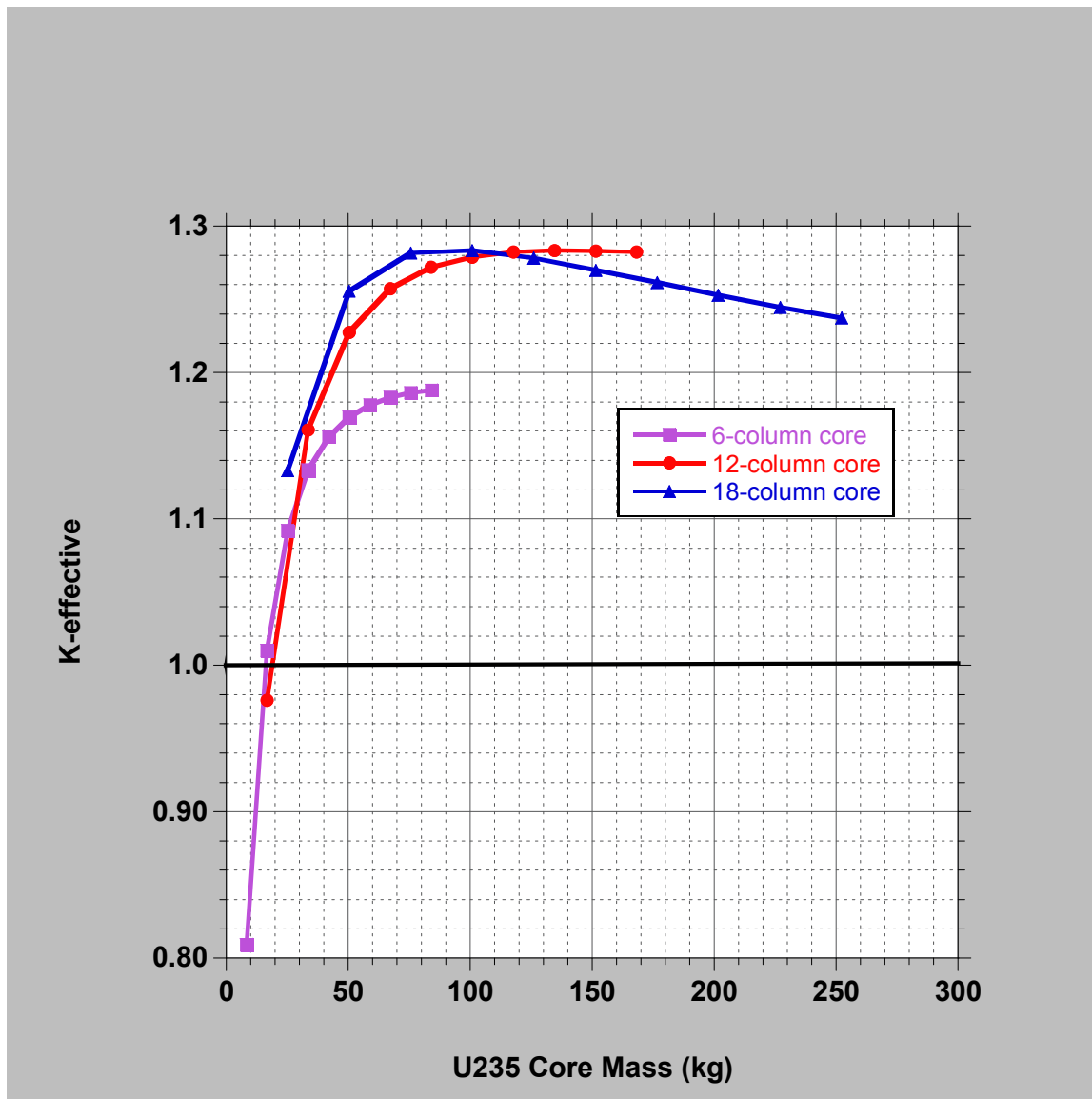


Figure 2-5. K-effective versus the total U-235 core mass loading for the three core configurations.

Although these numbers are very rough, it shows that there is probably plenty of room for all three cores to achieve a 1-year cycle with reasonable PFs. And for the 12- and 18-column cores, substantially longer cycles and/or higher core powers could be realized that in turn would increase exposure time, capacity factor, or irradiation fluxes, all goals for an optimized test reactor.

One additional criticality study was performed to better understand the reactivity consequences of maintaining the 0.6225 cm fuel rod radius from the FSV fuel block. K-effective was calculated as a function of PF for different fuel rod radii (0.6225, 0.55, 0.50, and 0.40 cm). Figure 2-6 is a plot of k-effective versus PF and fuel rod radius.

As the fuel rod radius is decreased, the core k-effective increases, and increases substantially for the higher PFs, as noted by the upward shift in the curves. In addition, the curves shift to the right or to higher PFs for decreasing fuel rod radius. For PFs > 25%, k-effective clearly increases with decreasing fuel rod radius. For example, at a PF = 30%, k-effective increases from 1.31 to 1.37. Therefore, maintaining the FSV lattice pitch, but reducing the fuel rod radius, may allow for a boost in core reactivity.

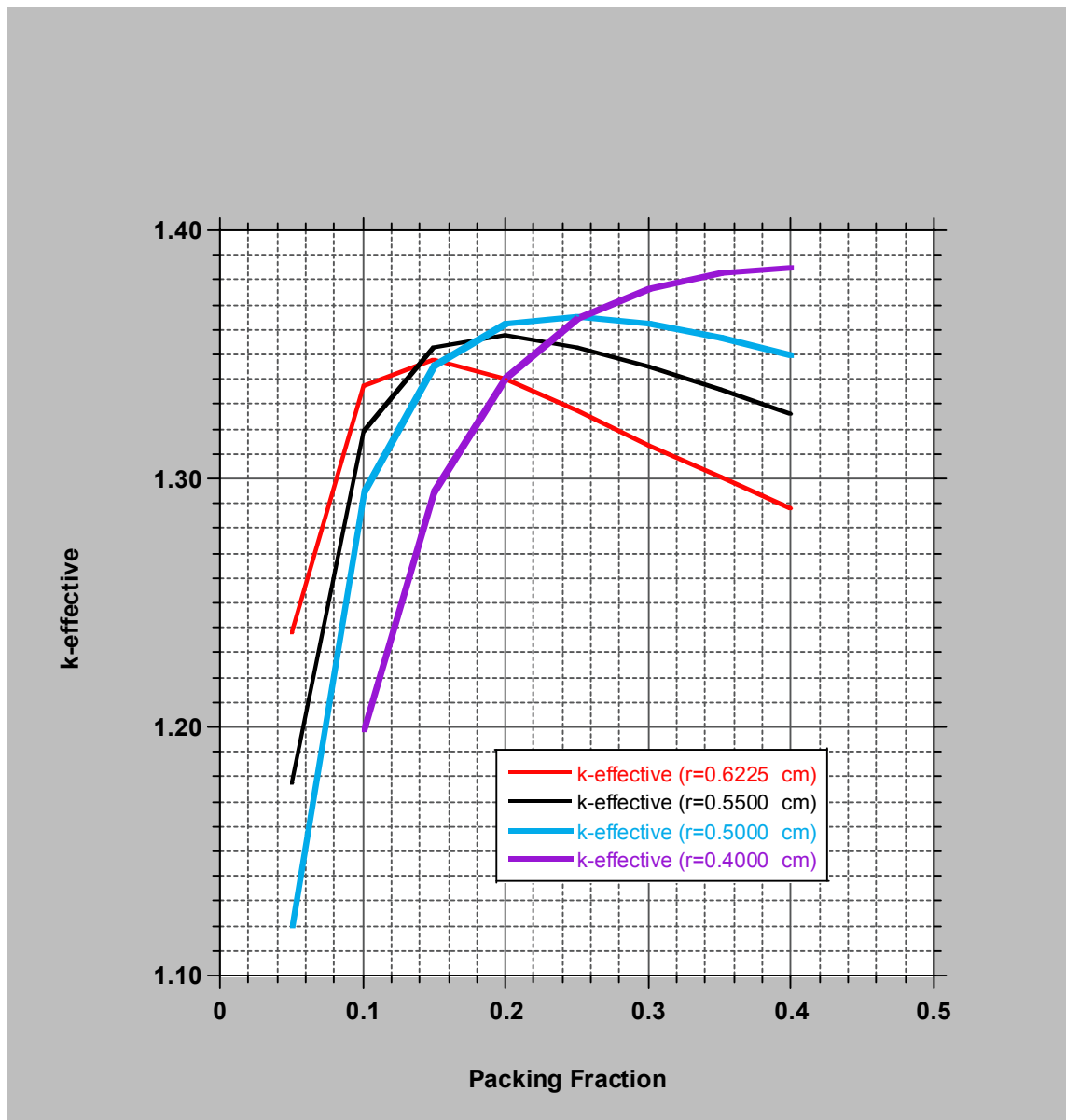


Figure 2-6. K-effective versus packing fraction and fuel rod radius for the 18-column core.

The triangular lattice pitch and fuel rod radius in the FSV block is typically under-moderated for prismatic core PFs and corresponding U-235 block loadings. Decreasing the fuel rod radius increases the neutron moderation and gives a boost to core reactivity. Therefore, the fuel rod radius could be an optimization parameter in future block and core designs. The loss in uranium block loading due to a reduction in fuel rod radius would need to be balanced against PF, cycle length, and core power.

2.4 Irradiation Total Flux

The magnitude of the total irradiation flux is presented for the three core configurations. Spectral data have yet to be reduced to give fast and thermal fluxes. For each core configuration, three radial locations

in the core were assessed for the total flux: (1) central irradiation hole at core center, (2) coolant channels in the middle of fuel blocks, and (3) outer reflector irradiation holes. The total irradiation fluxes are calculated parametrically as a function of PF and normalized to a total core power of 100 MW. Tables 2-1, 2-2, and 2-3 give the total calculated irradiation flux for the 6, 12, and 18-column active core configurations.

Table 2-1. Maximum total flux for the 6-column core at select locations in the core.

| PF | k-effective ^a | Central (Ring 1) | Fuel Block (Ring 2) | Fuel Block (Ring 3) | Outer Reflector (Ring 3) |
|------|--------------------------|------------------|---------------------|---------------------|--------------------------|
| 0.05 | 0.808965 | 6.20E+14 | 1.30E+15 | -- | 9.64E+14 |
| 0.10 | 1.010279 | 4.30E+14 | 7.96E+14 | -- | 6.06E+14 |
| 0.15 | 1.092266 | 3.66E+14 | 6.23E+14 | -- | 4.86E+14 |
| 0.20 | 1.133378 | 3.36E+14 | 5.04E+14 | -- | 4.28E+14 |
| 0.25 | 1.156001 | 3.16E+14 | 4.88E+14 | -- | 3.93E+14 |
| 0.30 | 1.169602 | 3.03E+14 | 4.52E+14 | -- | 3.69E+14 |
| 0.35 | 1.177733 | 2.92E+14 | 4.25E+14 | -- | 3.51E+14 |
| 0.40 | 1.182875 | 2.86E+14 | 4.08E+14 | -- | 3.39E+14 |
| 0.45 | 1.186067 | 2.80E+14 | 3.91E+14 | -- | 3.28E+14 |
| 0.50 | 1.187994 | 2.75E+14 | 3.78E+14 | -- | 3.19E+14 |

a: relative error ≤ 0.00005

Table 2-2. Maximum total flux for the 12-column core at select locations in the core.

| PF | k-effective ^a | Central (Ring 1) | Fuel Block (Ring 2) | Fuel Block (Ring 3) | Outer Reflector (Ring 4) |
|------|--------------------------|------------------|---------------------|---------------------|--------------------------|
| 0.05 | 0.975936 | 1.22E+14 | -- | 6.00E+14 | 4.14E+14 |
| 0.10 | 1.160856 | 8.05E+13 | -- | 3.66E+14 | 2.61E+14 |
| 0.15 | 1.227395 | 6.71E+13 | -- | 2.89E+14 | 2.11E+14 |
| 0.20 | 1.257359 | 6.05E+13 | -- | 2.49E+14 | 1.85E+14 |
| 0.25 | 1.271789 | 5.68E+13 | -- | 2.27E+14 | 1.71E+14 |
| 0.30 | 1.278976 | 5.38E+13 | -- | 2.10E+14 | 1.60E+14 |
| 0.35 | 1.282243 | 5.22E+13 | -- | 1.98E+14 | 1.53E+14 |
| 0.40 | 1.283248 | 5.06E+13 | -- | 1.89E+14 | 1.47E+14 |
| 0.45 | 1.283037 | 4.95E+13 | -- | 1.82E+14 | 1.43E+14 |
| 0.50 | 1.282236 | 4.87E+13 | -- | 1.76E+14 | 1.39E+14 |

a: relative error ≤ 0.00005

Table 2-3. Maximum total flux for the 18-column core (baseline) at select locations in the core.

| PF | k-effective ^a | Central (Ring 1) | Fuel Block (Ring 2) | Fuel Block (Ring 3) | Outer Reflector (Ring 4) |
|------|--------------------------|------------------|---------------------|---------------------|--------------------------|
| 0.05 | 1.133139 | 1.88E+14 | 4.50E+14 | 3.71E+14 | 2.70E+14 |
| 0.10 | 1.255744 | 1.41E+14 | 2.87E+14 | 2.41E+14 | 1.81E+14 |
| 0.15 | 1.281518 | 1.27E+14 | 2.33E+14 | 1.98E+14 | 1.54E+14 |
| 0.20 | 1.283496 | 1.19E+14 | 2.06E+14 | 1.78E+14 | 1.40E+14 |
| 0.25 | 1.278097 | 1.14E+14 | 1.88E+14 | 1.65E+14 | 1.32E+14 |
| 0.30 | 1.269855 | 1.11E+14 | 1.76E+14 | 1.56E+14 | 1.27E+14 |
| 0.35 | 1.261387 | 1.09E+14 | 1.68E+14 | 1.51E+14 | 1.24E+14 |
| 0.40 | 1.252899 | 1.07E+14 | 1.61E+14 | 1.46E+14 | 1.21E+14 |
| 0.45 | 1.244678 | 1.05E+14 | 1.55E+14 | 1.42E+14 | 1.20E+14 |
| 0.50 | 1.237144 | 1.03E+14 | 1.50E+14 | 1.39E+14 | 1.18E+14 |

a: relative error ≤ 0.00005

The central irradiation facility, or hole, is located at the center of the core in Ring 1. This facility is currently modelled as a stainless steel tube with a 15.0 cm (5.91 in.) outer diameter and a wall thickness of 1.785 cm (0.70 in.). Inside the tube is a helium-filled vertical hole (central irradiation facility) with a diameter of 11.43 cm (4.50 in.). The maximum calculated flux in all irradiation holes is near the middle of Level 5 or above core midplane (temperature effect). For the central irradiation hole, each level of the hole is further segmented into 12 axial segments, so the maximum calculated flux value in the central irradiation hole is relatively accurate.

The second irradiation facility locations considered are coolant channels in the middle of fuel blocks. Specific irradiation holes in fuel blocks are not currently modelled, but the coolant channels near the center of the fuel block provided easy-to-tally locations that would be comparable to dedicated irradiation holes. The calculated flux values in these coolant channels is an average over the coolant channel length for each axial fuel block or level. The maximum flux value will therefore be higher than the average value quoted in the table data here.

The six outer reflector block irradiation facilities are located in the graphite block ring just beyond the last fuel ring. For the 6-column core, these facilities are located in the graphite block ring 3 and in the 12- and 18-column cores in the graphite block ring 4. There are six irradiation facilities uniformly spaced around this first outer reflector block ring. These facilities are currently modelled as vertical helium-filled holes with a diameter of 10.16 cm (4.00 inches). The holes are located very close to the edge of the fuel blocks. Also, these holes currently do not include a stainless steel tube like the center test facility. The maximum calculated flux in these holes is also from Level 5. Each level is further segmented into 12 axial segments, so the maximum calculated flux value in these irradiation holes is relatively accurate.

Note that for the lowest PF, some core configurations are not critical.

Comparison of the maximum irradiation total flux results in Tables 2-1, 2-2, and 2-3 shows several interesting trends that will be useful in future designs and design evaluations. The first trend observed is the smaller the number of fuel columns in the core, the greater the flux. This is because the 100 MW total core power is compacted into fewer fuel blocks, requiring a higher fission rate and flux to maintain power.

A second trend is the PF. As the PF decreases in all three cores, the flux increases. The decrease in PF or the decrease in the number of U-235 atoms must be balanced by the product of the fission cross section and flux to maintain power. In general, this trend will always lead to an increase in the flux.

A third observation is that the central irradiation facility has a slightly lower flux than the outer graphite reflector irradiation facilities. At first glance this seems unusual, but can be explained by the closer proximity of the outer reflector block holes to a fuel block and the fact that these holes are in the thermal neutron peak region in the outer reflector. Plus, currently no stainless steel tubes are modeled in these holes to absorb thermal and epi-thermal neutrons and reduce flux.

A fourth observation is that the highest total fluxes are in the middle of the fuel blocks. This observation would seem to provide the impetus to place irradiation facilities at the center of fuel block columns. However, the total flux spectral content will first have to be evaluated. An irradiation hole in the middle of a fuel block will be relatively hard with a 1:1 fast-to-thermal ratio with only 23% of the total flux being thermal neutrons ($E < 2.0$ eV), whereas the outer reflector holes will have a much softer spectrum with a 1:7 fast-to-thermal ratio and approximately 66% of the total flux being thermal neutrons ($E < 2.0$ eV).

The total flux in the Advanced Gas Reactor (AGR)-3/4 fuel experiment in the northeast flux trap of the Advanced Test Reactor was typically $\leq 4.0E+14$ n/cm²/s. The baseline 18-column core exhibits total fluxes approximately a factor of four less than this value in both the central and outer reflector positions, and a factor of three less in the harder spectrum fuel blocks. The total flux in the compact 6-column core in the outer reflector positions, however, looks very promising.

2.5 Power-Peaking

An important factor to consider when evaluating the three core configurations is fuel rod or compact power-peaking. In the three core configurations considered, all are annular cores and fuel rod power-peaking naturally occurs on the core-reflector interfaces.

Using the MCNP core models, it is possible to calculate the relative fuel rod power in every fuel block throughout the core and derive a peak-to-average value for each fuel rod. Table 2-4 gives the maximum peak-to-average value in each core as a function of PF. These maximum values occur exclusively on the core-reflector interface; for 12-column core, the maximum powered fuel rod is at the inner core-reflector interface and for the 6-column and 18-column cores, the maximum powered fuel rod is at the outer core-reflector interface at a fuel block corner.

Table 2-4. Fuel rod maximum peak-to-average power.

| PF | 6-column core | 12-column core | 18-column core |
|------|---------------|----------------|----------------|
| 0.05 | 1.48 | 1.61 | 1.41 |
| 0.10 | 1.60 | 1.73 | 1.59 |
| 0.15 | 1.71 | 1.85 | 1.76 |
| 0.20 | 1.82 | 1.97 | 1.91 |
| 0.25 | 1.92 | 2.08 | 2.05 |
| 0.30 | 2.01 | 2.17 | 2.19 |
| 0.35 | 2.09 | 2.26 | 2.23 |
| 0.40 | 2.18 | 2.35 | 2.43 |
| 0.45 | 2.26 | 2.43 | 2.54 |
| 0.50 | 2.33 | 2.51 | 2.57 |

Power peaking will be mitigated with burnable poisons, PF grading, and control rod insertions.

2.6 Average Particle Power

Particle power is also an important parameter to consider. Excessive particle powers lead to excessive kernel burnups and particle temperatures leading to potential particle failures. Balancing particle, compact, and fuel rod power throughout the core will lead to a more uniform burnup and temperature distribution extending particle in-core life and integrity. Although high-powered fuel rods were identified in the previous section, it is useful at this stage to simply estimate the average particle power in the three core configurations. One can then apply the fuel rod power-peaking factors to estimate a maximum particle power. The mitigating effects of strategically placed burnable poisons, PF grading, and insertion of control rods have not yet been considered. TRISO fuel particle powers are typically limited to ≤ 400 mW.

The three core configurations have widely varying numbers of fuel blocks in the core, namely, 48, 96, and 144 for the 6-, 12-, and 18-column core configurations, respectively. Fuel block powers must go up as the number of fuel blocks in the core decreases, while at the same time holding the total core power constant (100 MW). Higher fuel block powers translate directly into higher compact and TRISO fuel particle powers. For the average particle power estimates, the total core power is divided by the total number of TRISO fuel particles in the core using the total number of compacts in the core and PF. Tables 2-5, 2-6, and 2-7 give the average particle powers for the three cores.

As expected, the particle powers decrease with increasing PF. The greater the number of particles in the core, the lower the power load on the average particle. This is also confirmed by the fact that the 6-column core has the highest average particle powers of the three cores; the 400 mW limit being exceeded at PF=0.05.

Table 2-5. Average TRISO fuel particle power estimates in the 6-column core.

| PF | Total Number of Particles in Core | Particle Power (mW/particle) |
|------|-----------------------------------|------------------------------|
| 0.05 | 1.3534E+08 | 739 |
| 0.10 | 2.7069E+08 | 369 |
| 0.15 | 4.0603E+08 | 246 |
| 0.20 | 5.4137E+08 | 185 |
| 0.25 | 6.7672E+08 | 148 |
| 0.30 | 8.1206E+08 | 123 |
| 0.35 | 9.4740E+08 | 106 |
| 0.40 | 1.0827E+09 | 92 |
| 0.45 | 1.2181E+09 | 82 |
| 0.50 | 1.3534E+09 | 74 |

Table 2-6. Average TRISO fuel particle power estimates in the 12-column core.

| PF | Total Number of Particles in Core | Particle Power (mW/particle) |
|------|-----------------------------------|------------------------------|
| 0.05 | 2.7069E+08 | 369 |
| 0.10 | 5.4137E+08 | 185 |
| 0.15 | 8.1206E+08 | 123 |
| 0.20 | 1.0827E+09 | 92 |
| 0.25 | 1.3534E+09 | 74 |
| 0.30 | 1.6241E+09 | 62 |
| 0.35 | 1.8948E+09 | 53 |
| 0.40 | 2.1655E+09 | 46 |
| 0.45 | 2.4362E+09 | 41 |
| 0.50 | 2.7069E+09 | 37 |

Table 2-7. Average TRISO fuel particle power estimates in the 18-column core.

| PF | Total Number of Particles in Core | Particle Power (mW/particle) |
|------|-----------------------------------|------------------------------|
| 0.05 | 4.0603E+08 | 246 |
| 0.10 | 8.1206E+08 | 123 |
| 0.15 | 1.2181E+09 | 82 |
| 0.20 | 1.6241E+09 | 62 |
| 0.25 | 2.0301E+09 | 49 |
| 0.30 | 2.4362E+09 | 41 |
| 0.35 | 2.8422E+09 | 35 |
| 0.40 | 3.2482E+09 | 31 |
| 0.45 | 3.6543E+09 | 27 |
| 0.50 | 4.0603E+09 | 25 |

Perhaps the most important observation is that the average particle powers are all <200 mW for $PF \geq 0.20$ and comfortably below the 400 mW limit for all three cores. Of course, applying the fuel power-peaking factors to these powers push some particle powers close to the limit, but judicious placement of burnable poisons has been shown previously to bring even the worst power-peaking fuel rods down to ~ 1.20 power-peaking factors over an entire 1.5-year cycle.

Relative to particle power, the PF parameter variable provides good flexibility in the design of the test reactor.

3. Thermal Hydraulics

The thermal behavior of the reactor is being simulated using the RELAP5-3D computer code (RELAP5-3D Code Development Team, 2014). The input model includes the reactor vessel and internals, the reactor cavity, and a simplified reactor cavity cooling system (RCCS). Steady state and transient calculations were performed using the model; sensitivity calculations were also performed to investigate different core configurations.

3.1 Input Model Description

The RELAP5-3D input model includes the primary structures and flow paths within the reactor vessel; a nodalization diagram is shown in Figure 3-1. A cross section of the 18-column core was presented in Figure 1-1 and is the basis for the RELAP5-3D model. Component 100 represents the vessel inlet region, Component 110 is the annulus between the core barrel and reactor vessel, and Component 120 is the upper plenum region. A number of parallel flow paths are modeled between the upper and lower plenum (Component 195): fuel block coolant holes (Components 140 and 150), the gaps between the hexagonal blocks (Components 135, 145, 155, 175, and 185), the gap between the PSR and the core barrel (Component 190), the gap between the center irradiation tube and the central reflector block (Component 130), and the gaps around the control rods and irradiation tubes in the first ring of the side reflector (Component 170).

The fuel blocks are modeled using unit cells centered on the coolant holes, with a cylindrical graphite structure around the hole preserving the graphite mass in the block. The fuel rods are modeled as solid cylinders with a helium annulus between them and the graphite, with radiation modeled between the fuel rod and the graphite. Separate heat structures model the central reflector, outer reflector rings, and the PSR. The core barrel and reactor vessel cylinder and upper head are included in the model, as are the upper plenum shield, some upper plenum internals, and the floor of the lower plenum.

The center irradiation loop is modeled as an 11.43-cm diameter (outer) tube with a 2.54-mm gap around it. The control rod and irradiation loop holes in the outer reflector are all assumed to have diameters of 10.16 cm with a control rod or flow tube outer diameter of 8.89 cm.

In the outer reflector inner ring, the holes in the blocks to accommodate control rods and irradiation tubes have a diameter of 10.2 cm. The control rods and tubes in the holes have an outer diameter of 8.89 cm, leaving a gap of 6.55 mm.

A thin layer of graphite was modeled on the surface of the fuel blocks. This structure was needed to allow the graphite to have convective heat transfer to the coolant channels, the helium gap around the fuel rods, and the helium gap between adjacent fuel blocks. This structure is in a conduction enclosure with the same surface as the coolant channels, and in a radiation enclosure that includes the fuel blocks and the central and outer reflector blocks in the rings adjacent to the fueled rings. The conduction area factor for this thin layer was made as large as practical to keep its temperature as close to that of the graphite next to it as possible, but not so large that numerical instabilities were encountered.

The RCCS is modeled as flat panels facing the reactor vessel, arranged in a square whose side length is twice the vessel diameter and whose height is slightly larger than that of the reactor vessel. Cooling water flows on the inside of the panels, with the back side (away from the vessel) having an insulated boundary. The flow is driven by natural convection, with a large water volume above the panels providing colder water to the bottom of the panels and accepting the heated water as it exits the RCCS panels. The space between the vessel and the RCCS panels is modeled as a large air-filled volume.

Control systems are used to establish steady state conditions. The outlet pressure is controlled to provide a vessel inlet pressure of 7.0 MPa, and the coolant flow rate is controlled to provide a coolant temperature of 750°C in the lower (outlet) plenum. A flat axial and radial power profile was modeled in the fuel.

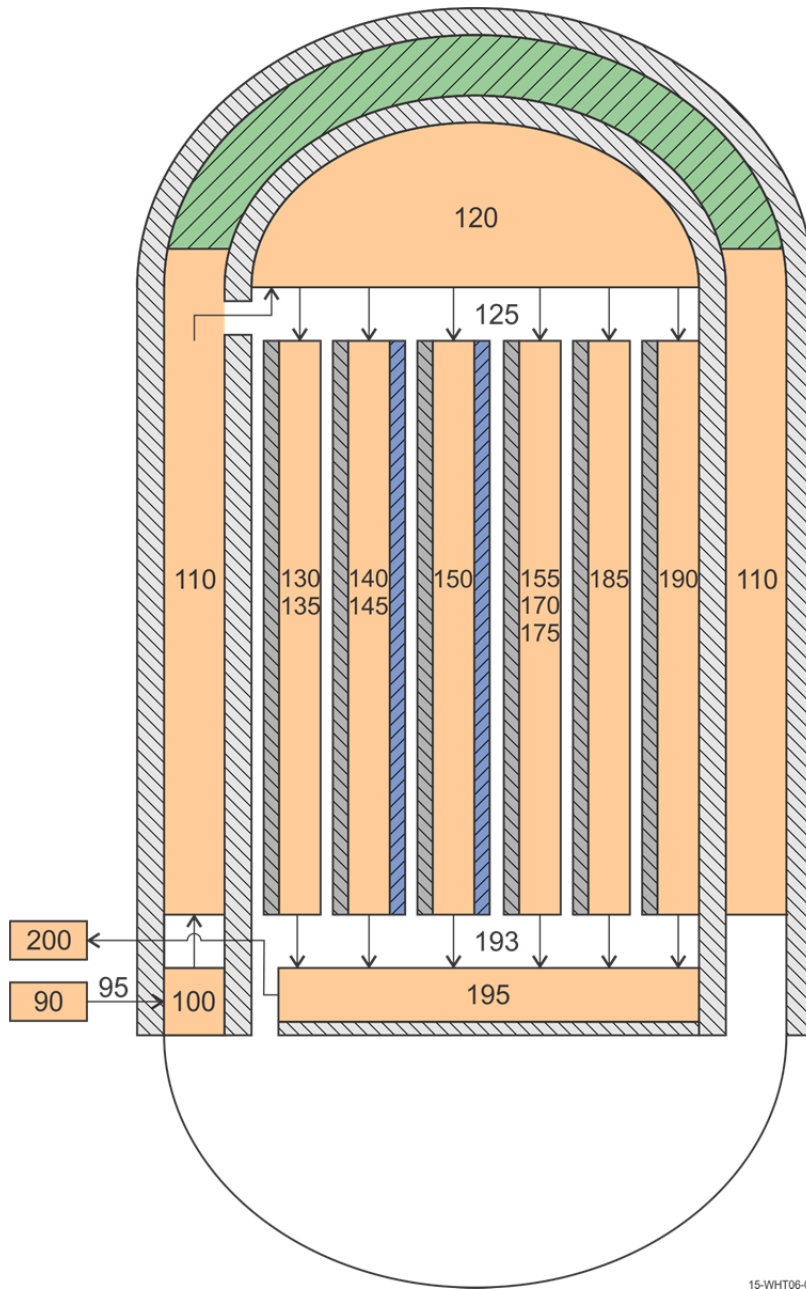


Figure 3-1. Nodalization of the reactor vessel for the gas test reactor RELAP5-3D input model.

3.2 Steady State Simulations

Calculations have been performed to determine the steady state conditions in the reactor vessel. Scoping sensitivity calculations were performed to address different irradiation loop sizes and contents. Sensitivity calculations were also performed to investigate the flow in the gaps between the blocks and the effects of reflector heating.

3.2.1 Scoping Sensitivity Studies

These simulations were performed using a simple core model with only fuel and reflector blocks, with no control rod or irradiation holes in the outer reflector. These calculations addressed the effect of different diameter fuel rods and the size of the irradiation loop in the center of the core and the gas gap around it. In all of the calculations, the core power was 100 MW with flat axial and radial power profiles. The gap between blocks was 1.0 mm. The coolant inlet and outlet temperatures were 350°C and 750°C, respectively.

3.2.1.1 Fuel Rod Diameter

Fuel rod diameters of 11.0, 11.5, 12.0, and 12.5 mm were modeled. The size of the fuel rod holes in the core blocks had a constant diameter of 12.7 mm.

The fuel temperatures in the two rings of fuel were within a few degrees of each other. Table 3-1 presents the axial fuel temperatures in the inner fueled ring for the four cases. The fuel temperatures decreased as the diameter increased because there was more fuel volume available for the same amount of power. The effect on the reflector temperatures was small, indicating that nearly all of the power is being removed by convection in the coolant channels, with only a small portion being radiated to the reflectors.

Table 3-1. Inner core ring fuel rod average temperatures from the fuel rod diameter sensitivity calculations.

| Core block | D = 11.0 mm | D = 11.5 mm | D = 12.0 mm | D = 12.5 mm |
|------------|-------------|-------------|-------------|-------------|
| 8 | 759°C | 715°C | 669°C | 648°C |
| 7 | 793°C | 750°C | 704°C | 678°C |
| 6 | 834°C | 794°C | 750°C | 720°C |
| 5 | 877°C | 839°C | 798°C | 765°C |
| 4 | 920°C | 885°C | 846°C | 810°C |
| 3 | 963°C | 930°C | 893°C | 850°C |
| 2 | 1005°C | 973°C | 935°C | 883°C |
| 1 | 1036°C | 1004°C | 964°C | 903°C |

3.2.1.2 Center Irradiation Tube

The size of the hole in the center of the central reflector block was varied first. For these calculations, a steel tube was assumed to be in close contact with the graphite reflector. The tube contained either water at typical pressurized water reactor conditions (15 MPa, 327°C) or molten salt (FLIBE) at 0.20 MPa and 547°C. Table 3-2 presents the results of these calculations; the basis for comparison was a solid graphite block.

Table 3-2. Center irradiation hole size sensitivity calculation results.

| Nominal Tube Size (in.) | Test Loop Fluid | Center Reflector T_{ave} (°C) | Change from Solid (°C) |
|-------------------------|-----------------|---------------------------------|------------------------|
| None | None | 645 | 0 |
| 3 | Water | 473 | -173 |
| 4 | Water | 458 | -187 |
| 3 | Molten salt | 594 | -51 |
| 4 | Molten salt | 589 | -56 |

The results showed that flow through the test loop reduced the average temperature of the central reflector graphite, and by quite a bit with a water loop. The temperature reduction is less with the molten salt because a higher loop temperature is needed to keep the salt molten. While the larger hole resulted in lower temperatures in the graphite, because there is less graphite to heat, the temperature difference is not considered significant.

The large reduction in temperature with a water loop may be a concern from the graphite standpoint, but it should be noted that there was no gap between the piping and the graphite block; a gap would be expected to be present in the reactor. Therefore, calculations were performed with different size gaps between the tube and the graphite. The gap contained helium flowing in parallel with the rest of the primary coolant flowing down through the core. Radiation was modeled between the flow tube and the graphite. Since the water loop had a greater impact, it was used as the base case.

Table 3-3 shows the results of these calculations. The average graphite temperature increased significantly with the gap modeled, with the presence of the gap being more significant than its size.

Table 3-3. Sensitivity on gap size around water-filled center irradiation tube.

| Nominal Tube Size (in.) | Gap around Tube (mm) | Center Reflector T_{ave} (°C) | Change from No Gap (°C) |
|-------------------------|----------------------|---------------------------------|-------------------------|
| 3 | 0.0 | 473 | 0 |
| 3 | 2.54 | 572 | 99 |
| 3 | 5.08 | 589 | 117 |
| 3 | 12.7 | 595 | 123 |
| 3 | 25.4 | 602 | 129 |
| 4 | 0.0 | 458 | 0 |
| 4 | 2.54 | 561 | 103 |
| 4 | 5.08 | 580 | 122 |
| 4 | 12.7 | 603 | 145 |
| 4 | 25.4 | 608 | 150 |

After these calculations were completed, it was noted that there is no Schedule 160 4-in. (10.2 cm) outside diameter piping; it was assumed that this piping grade will be used to accommodate high-pressure water. Subsequent analyses assumed a water-filled 4.5-in. (11.4 cm) outside diameter flow tube with a 2.54-mm. gap around it.

3.2.2 Steady State

Steady state calculations were performed using the input model described in Section 3.1. Two basic calculations were performed, one with and one without direct heating of the reflectors. These calculations assumed a 1-mm gap existed between all of the core and reflector blocks, a 2.54-mm gap around the 11.43-cm diameter center irradiation loop, and a 6.35-mm gap around the 8.89-cm diameter control rods or irradiation tubes in the side reflector. The center irradiation loop contains water at 15.0 MPa and 327°C, with a velocity of 5.0 m/s that makes the water essentially isothermal over the core height. The results of the steady state calculations are summarized in Table 3-4. Axial average temperatures in the table are over the height of the fueled length.

A little less than 2% of the total power is deposited directly in the reflectors in this simulation; it should be noted that there was no iteration between the physics and thermal-hydraulics to address how the changes in reflector temperatures would affect the neutron and gamma heating. The largest effect of the reflector heating was seen in the central reflector, whose temperature increased by nearly 100°C. Much smaller increases were calculated for the outer reflector rings. The peak and average fuel temperatures decreased less than 10°C.

3.2.3 Sensitivity Analyses

Several sensitivity studies were performed using the base input model described in Sections 3.1 and 3.2.2. They addressed core bypass flow and gap crossflow.

The size of the gap between blocks in the core will likely vary over time, as the graphite blocks shrink and expand as they are irradiated at elevated temperatures. The first set of calculations examined gap widths of 1.0, 1.5, 2.0, 2.5, and 3.0 mm.

Table 3-4. Steady state conditions.

| Parameter | No Reflector Heating | With Reflector Heating |
|-------------------------------------|----------------------|------------------------|
| Total power (MW) | 100 | 100 |
| Power in fuel (MW) | 100 | 98.2 |
| Coolant inlet temperature (°C) | 350 | 350 |
| Coolant outlet temperature (°C) | 750 | 750 |
| Primary coolant flow rate (kg/s) | 47.9 | 47.8 |
| Peak fuel temperature (°C) | 1048 | 1039 |
| Axial average temperature (°C) | | |
| Central reflector | 393 | 490 |
| Inner fuel ring graphite | 775 | 770 |
| Inner fuel ring fuel | 877 | 871 |
| Outer fuel ring graphite | 775 | 769 |
| Outer fuel ring fuel | 877 | 870 |
| Outer reflector Ring 4, inner half | 364 | 382 |
| Outer reflector Ring 4, outer half | 353 | 378 |
| Outer reflector Ring 5 | 351 | 368 |
| Permanent side reflector | 351 | 361 |
| Core barrel | 352 | 355 |
| Reactor vessel | 340 | 341 |
| RCCS heat removal (MW) | 0.51 | 0.51 |
| RCCS inlet temperature (°C) | 27 | 27 |
| RCCS flow rate (kg/s) | 125 | 125 |
| Reactor cavity air temperature (°C) | 111.5 | 111.5 |

The effect of these gaps on the core bypass flow and the peak fuel temperature are shown in Table 3-5. The bypass flow is defined as all coolant flow not passing through the coolant channels in the fuel blocks. While the peak fuel temperature increased as the bypass flow increased, because less coolant was flowing through the fuel block coolant channels, the increase was not very large.

Table 3-5. Block-to-block gap width sensitivity study results.

| Gap Width (mm) | Bypass Flow (%) | | | | Peak Fuel Temperature (°C) |
|----------------|---------------------|---------------------------|--------------------|-------|----------------------------|
| | Block-to-Block gaps | Tube and Control rod Gaps | PSR-to-Core Barrel | Total | |
| 1.0 | 3.2 | 8.0 | 4.6 | 15.9 | 995 |
| 1.5 | 5.2 | 7.9 | 4.6 | 17.7 | 1000 |
| 2.0 | 8.0 | 7.7 | 4.4 | 20.1 | 1012 |
| 2.5 | 11.3 | 7.5 | 4.3 | 23.1 | 1024 |
| 3.0 | 14.9 | 7.2 | 4.1 | 26.3 | 1039 |

One deficiency noted in the steady state results is the temperature difference between the gap flow channels around the fueled region. The modeling approach does not present a good method for attaching the gaps to both the fueled blocks and the adjacent ring of reflector blocks, which results in temperatures that are likely too hot in the core gap and too cold in the nearest reflector gaps. To try to increase the gap temperatures, crossflow connections were made at each axial level between the fuel region gap channel (Component 145) and the gap channels in the central reflector (Component 135) and the first ring of the side reflector (Component 155). The first calculation modeled the crossflow area based on a 3-mm gap between each of the blocks in the fuel rings. The second calculation increased this area by a factor of ten. The results of these steady state calculations are presented in Table 3-6, where it is seen that the increase in the reflector gap outlet temperatures was not very large and increasing the crossflow area had no effect.

Table 3-6. Effect of crossflow on gap outlet temperatures (°C).

| Coolant gap | Without Crossflow | With Smaller Crossflow | With Larger Crossflow |
|-----------------------------|-------------------|------------------------|-----------------------|
| Central reflector-to-Ring 2 | 598 | 599 | 599 |
| Ring 2-to-Ring 3 | 860 | 862 | 862 |
| Ring 3-to-Ring 4 | 470 | 482 | 482 |
| Ring 4-to-Ring 5 | 379 | 382 | 382 |
| Ring 5-to-PSR | 368 | 369 | 369 |
| PSR-to-core barrel | 369 | 369 | 369 |

3.3 Transient Simulations

Two simulations of a depressurized conduction cooldown (DCC) transient were performed to investigate the response of the system during a design-basis accident. Both calculations imposed a 5-s blowdown on the system. In Case 1, only the outlet plenum was open to atmospheric pressure, and a 5-s flow coastdown was imposed at the reactor vessel inlet. In Case 2, both the vessel inlet and outlet were open to atmospheric pressure, so that once-through flow through the core could occur. As will be seen in the figures, there was essentially no difference between the two cases. The transient simulations covered 7 days.

Figure 3-2 presents the peak fuel temperatures in the two fueled rings for both transient simulations. The temperatures dropped quickly at the beginning of the transient, as heat was redistributed from the bottom of the core toward the top; this is shown in Figure 3-3 for the inner core ring graphite. As the transient progressed, the peak fuel temperatures decreased continuously. Axial average fuel temperatures are presented in Figure 3-4. After the initial decrease following scram, a modest increase in temperature occurs, although the maximum temperatures are well below the steady state values.

Figures 3-5 through 3-7 show the radial temperature distribution across the reactor vessel heat structures. These temperatures are axial averages over the fueled length of the core. The central reflector and fuel ring temperatures peaked very early in the transient, and the peaks occurred progressively later moving radially outward from the center of the vessel, with the reactor vessel reaching its maximum temperature after about two days.

The power generated in the core and heat removed by the RCCS are shown in Figure 3-8. The powers were fairly well matched after about four days. Figure 3-9 presents the coolant temperature at the outlet of the RCCS. The small temperature change over the course of the transient indicates that there was more than enough flow in the RCCS to remove the heat reaching the surface of the cooling panels.

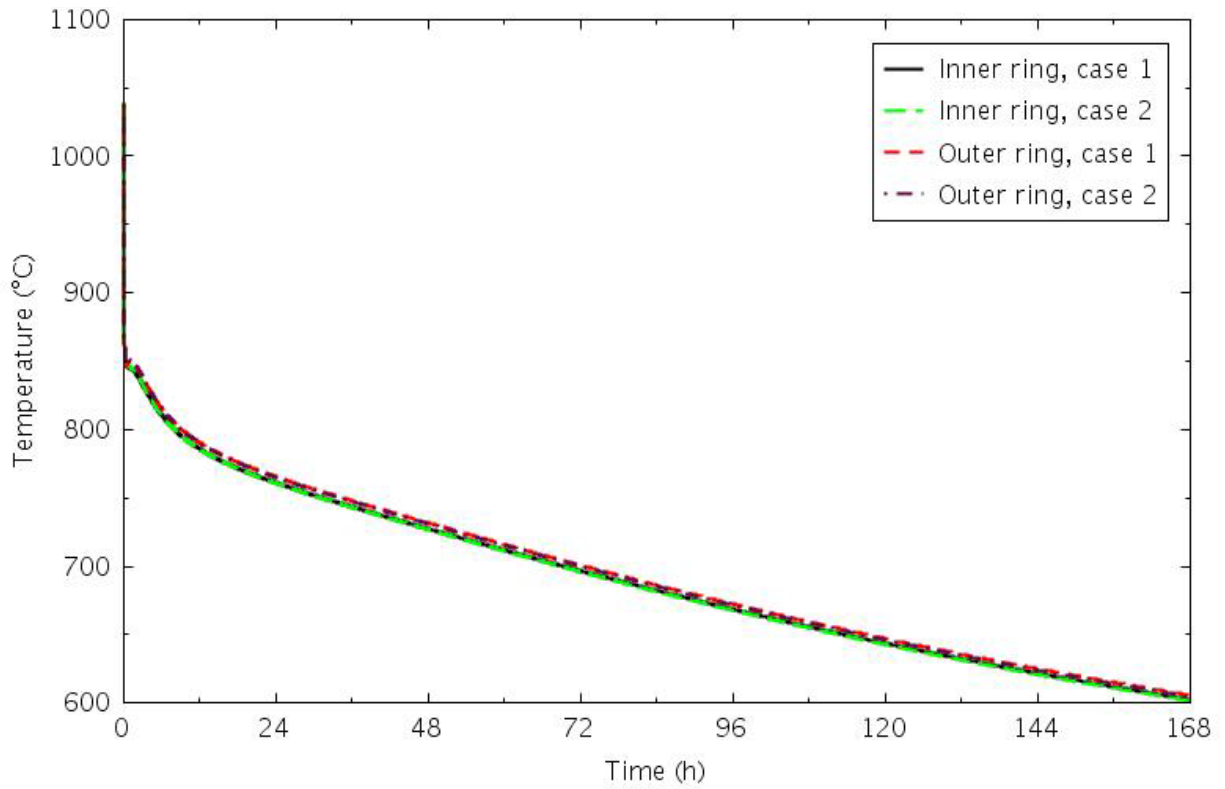


Figure 3-2. Peak fuel temperatures for the DCC transients.

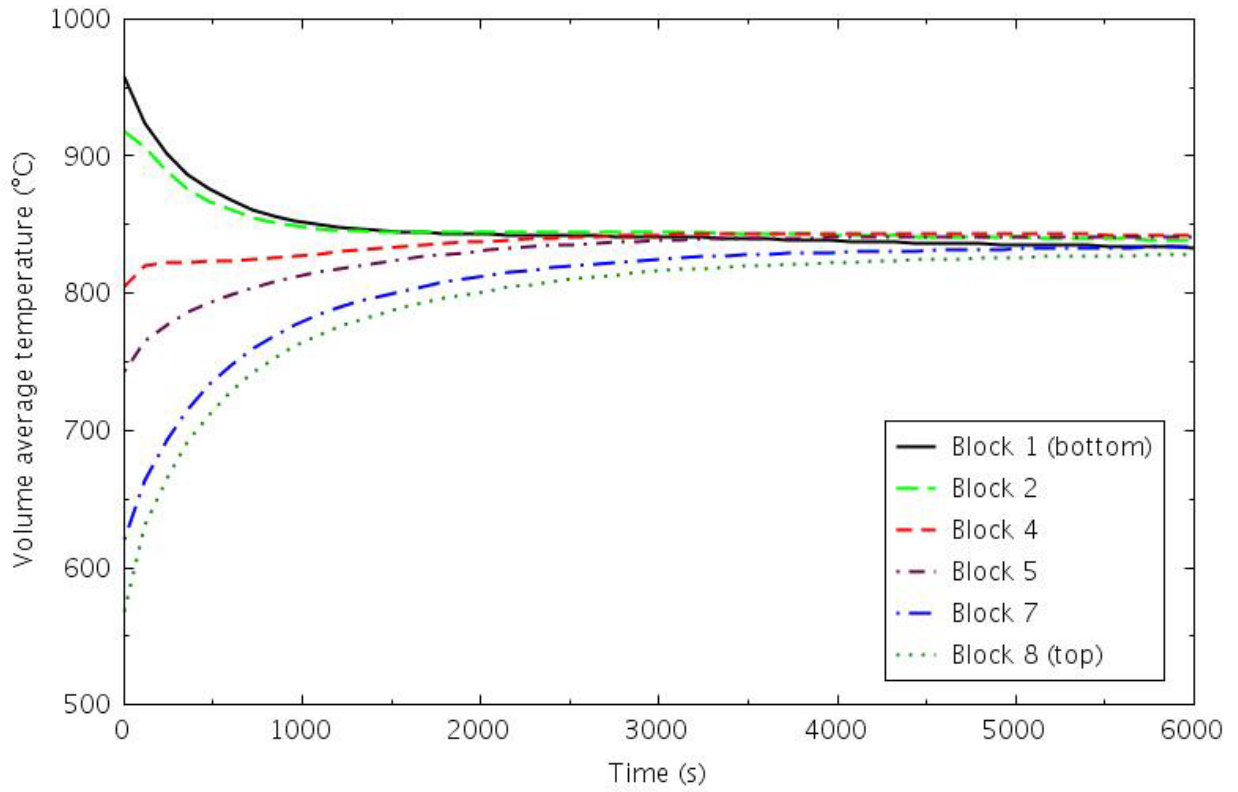


Figure 3-3. Axial temperature distribution in the inner fuel ring graphite for DCC transient Case 1.

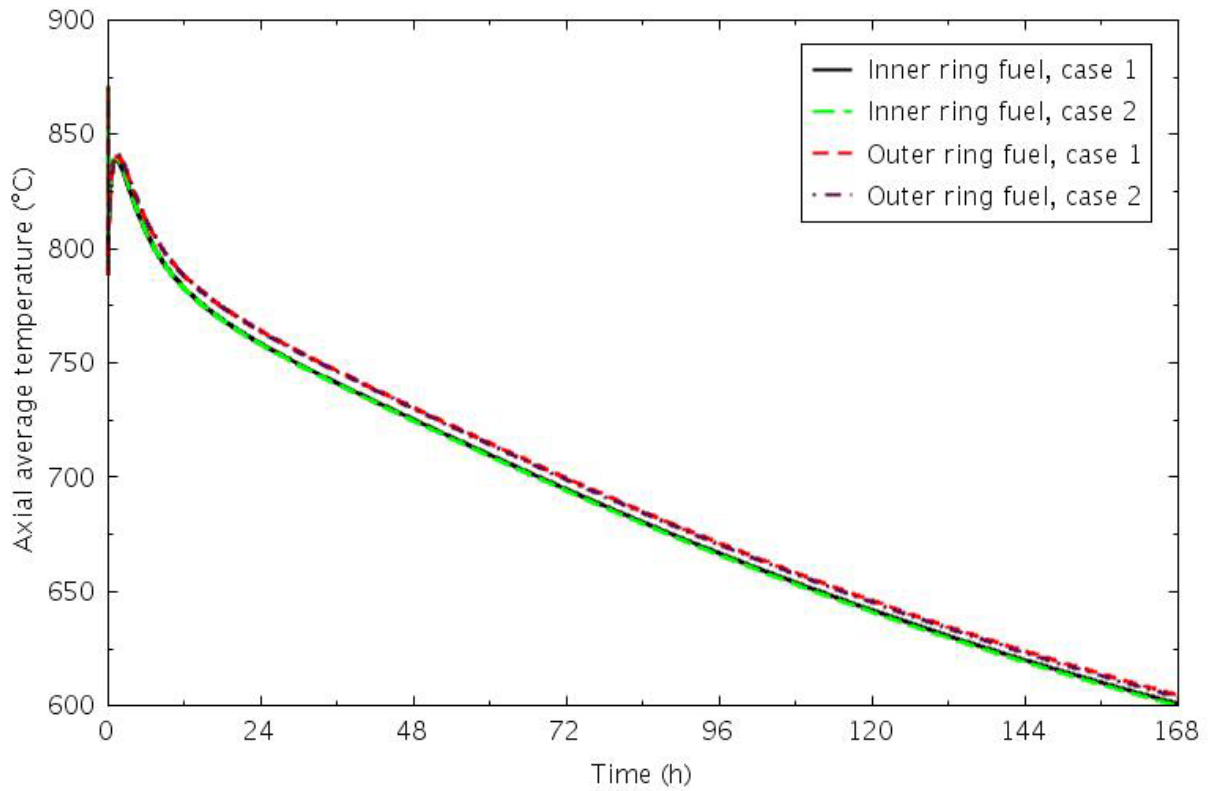


Figure 3-4. Average fuel temperatures for the DCC transients.

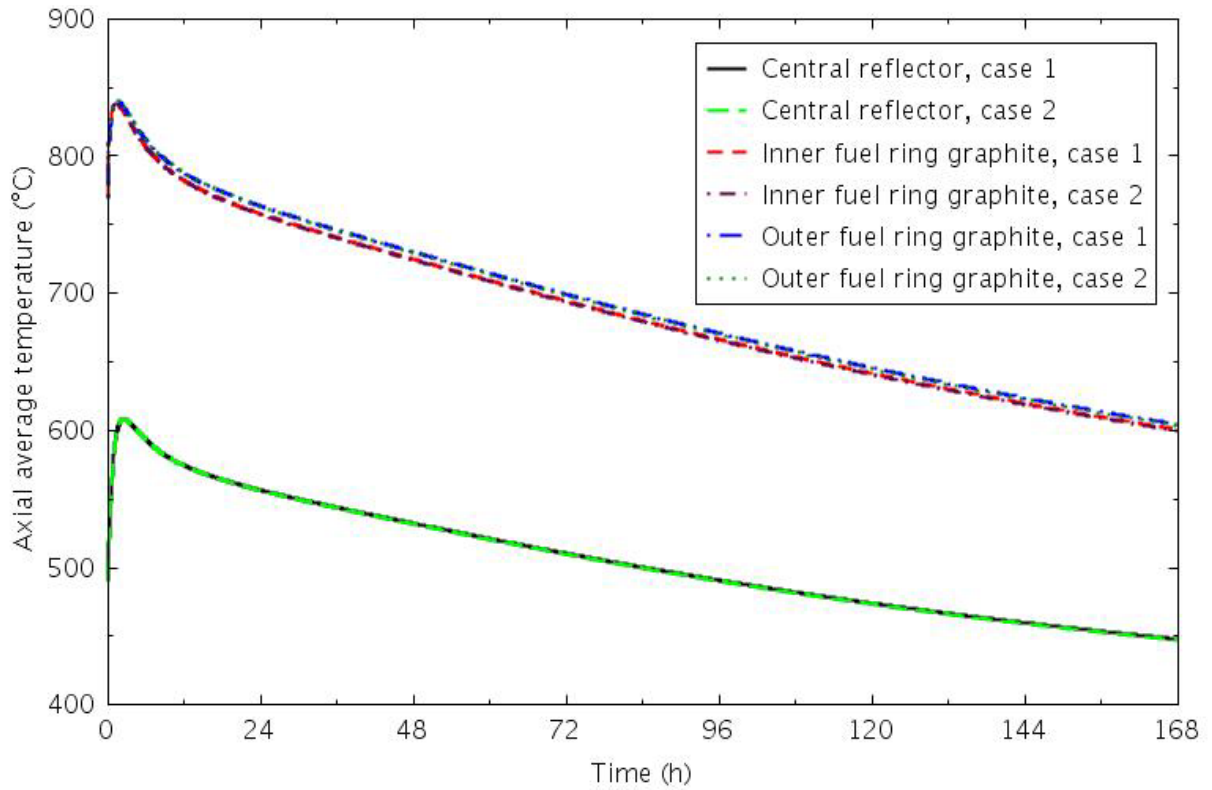


Figure 3-5. Temperatures in the central reflector and fuel ring graphite for the DCC transients.

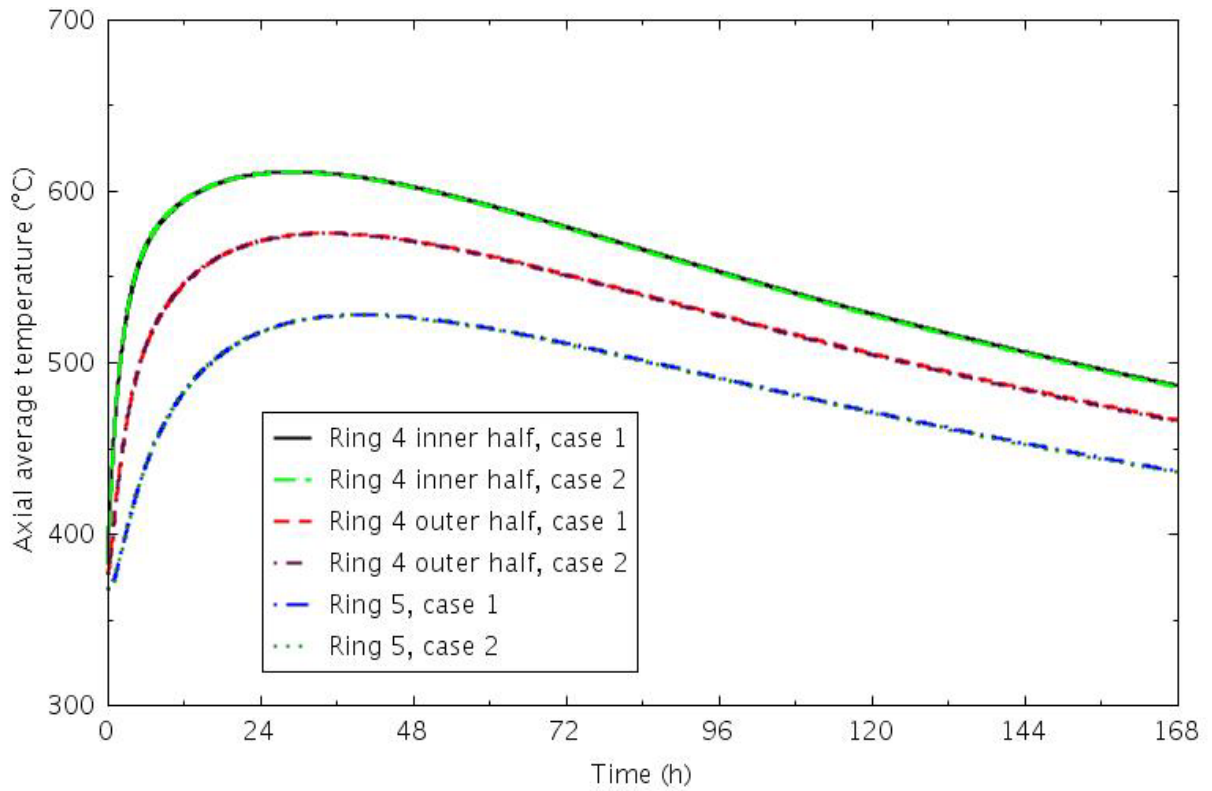


Figure 3-6. Temperatures in the outer reflector for the DCC transients.

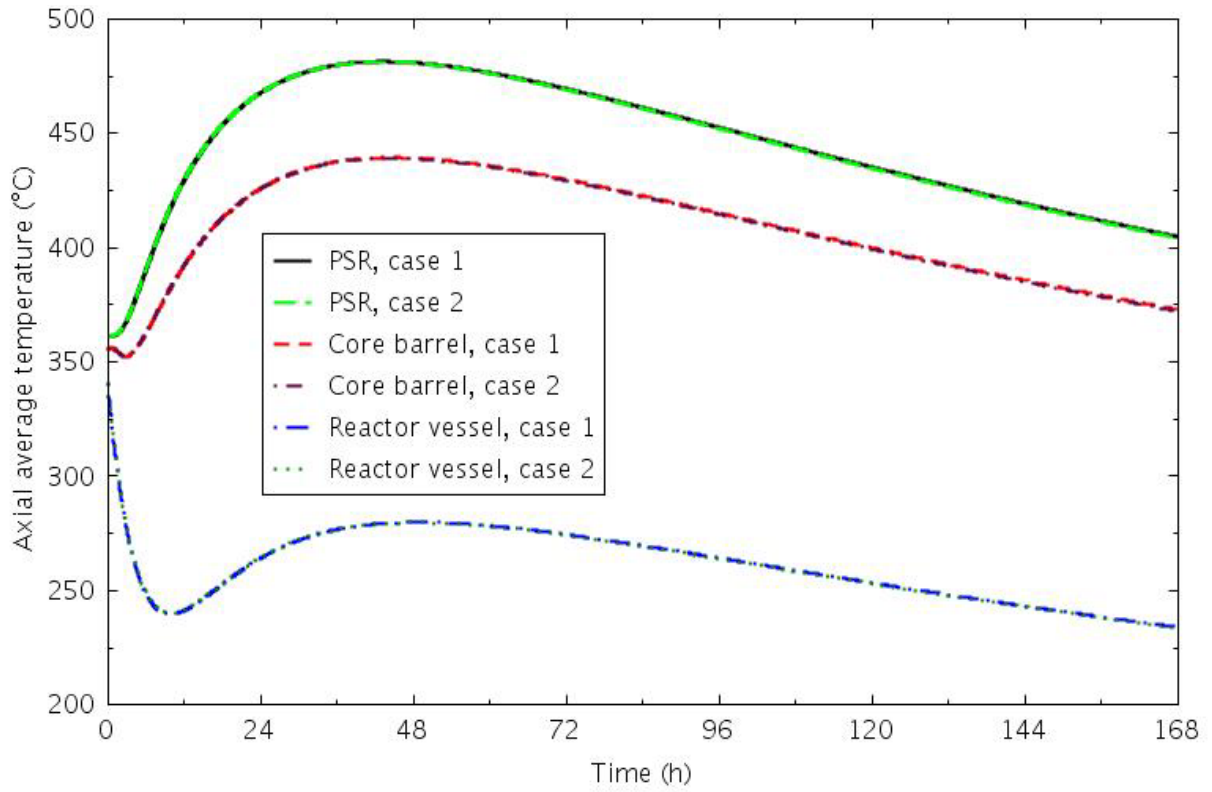


Figure 3-7. Temperatures in the PSR, core barrel, and reactor vessel for the DCC transients.

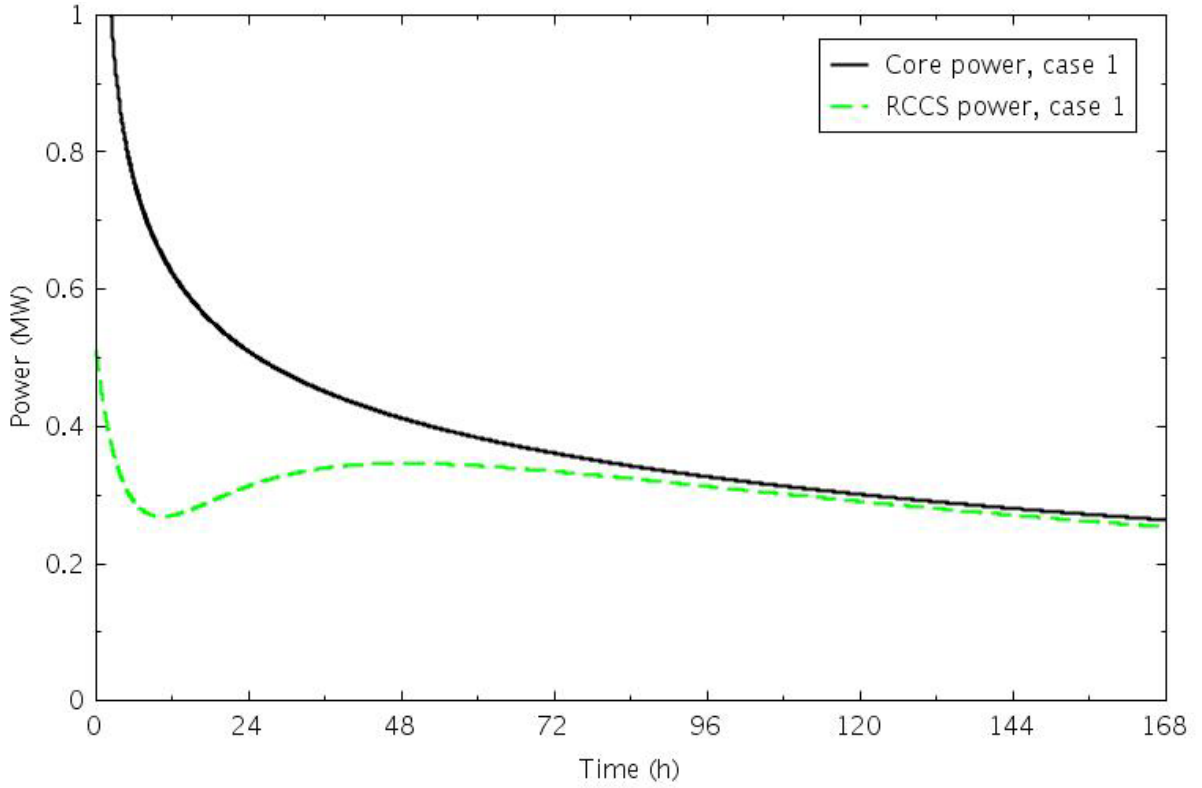


Figure 3-8. Core heat generation and RCCS heat removal for the DCC transients.

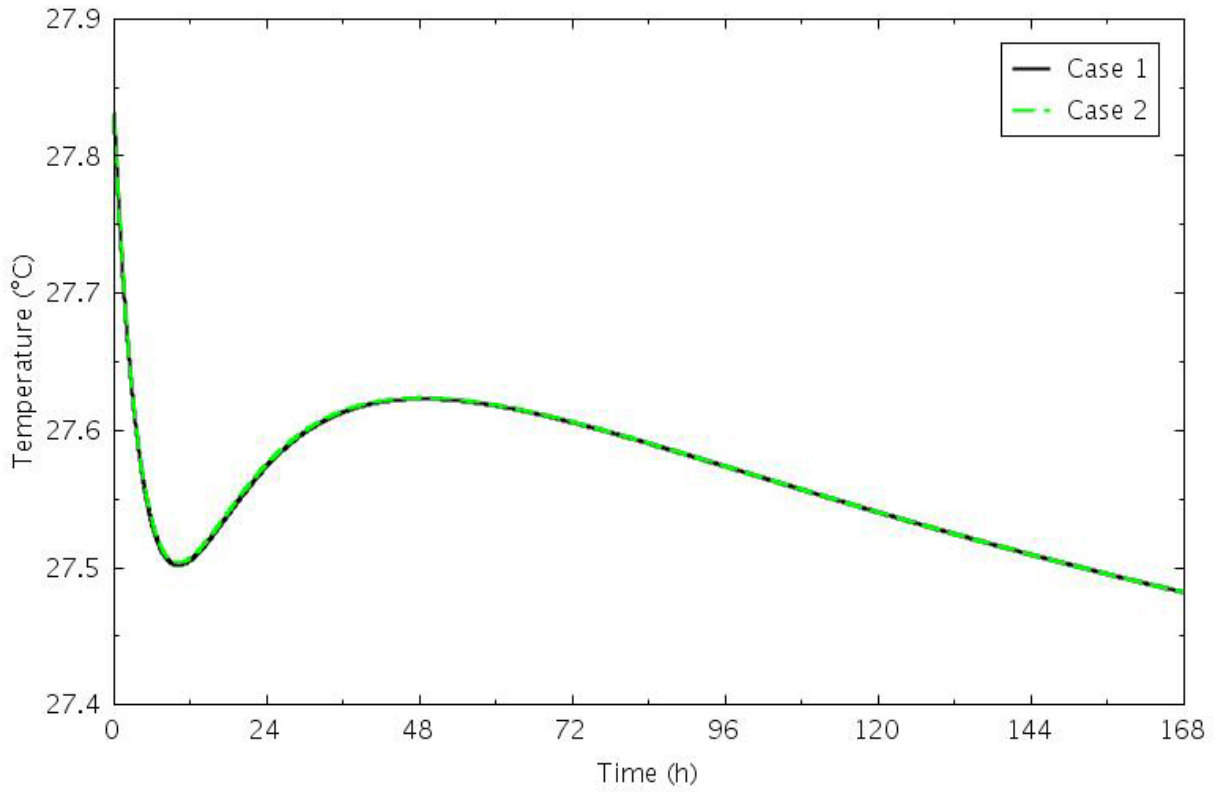


Figure 3-9. RCCS coolant outlet temperature for the DCC transients.

The temperature in the reactor cavity is presented in Figure3-10. No ventilation of the cavity was included in the model, so the steady state value is higher than would be expected in an operating facility.

Overall, the transient simulations showed a very coolable reactor. The heat from the fuel rings was quickly redistributed axially, then effectively removed radially. Peak fuel temperatures during the transient were lower than during steady state operation.

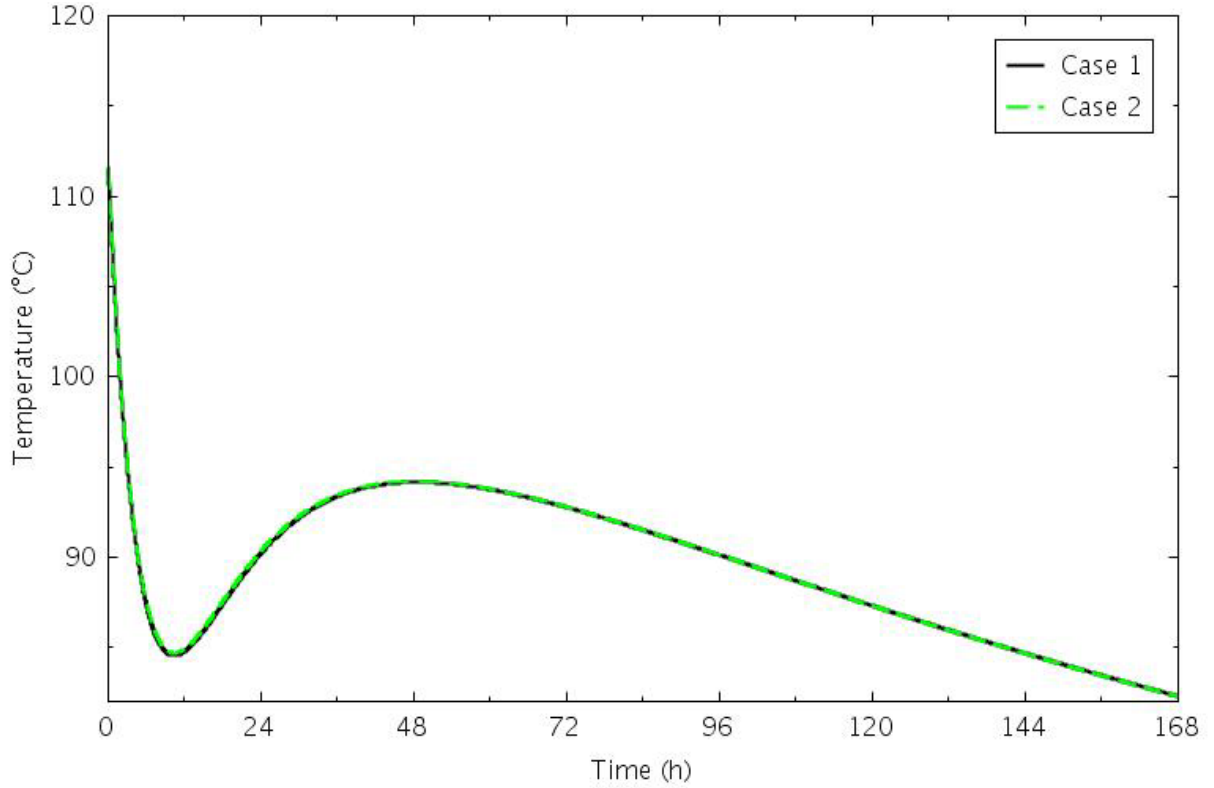


Figure 3-10. Reactor cavity gas temperature for the DCC transients.

4. Summary and Future Work

Some initial scoping calculations have been performed for a 100 MW gas-cooled test reactor. Reactor physics analyses have evaluated three core designs: the baseline 18-column core and two other single ring configurations, each of which appears to have sufficient reactivity to support a 1-year operating cycle; depletion calculations will be performed to provide a better estimate of the core life. The thermal-hydraulic analyses for the baseline 18-column core, or two-fueled ring model, showed that the steady state reflector temperatures are relatively cool, and that fuel temperatures during a depressurized conduction cooldown show very little increase from steady state values.

The baseline 18-column core design will work, but will be a relatively inefficient test reactor. A more efficient and higher flux core will be more compact with a higher power density and 6-10 fuel columns. A more compact core will, however, present more challenges in cooling the fuel, preventing excessive particle powers, and achieving a long cycle length. Boosting the core power above 100 MW will add to these design challenges. The new TRISO fuel particle designs greatly help in achieving higher fuel block loadings that should translate into relatively long cycle lengths (~1 year). Core optimization has several robust variables to aid in the design, most notably particle packing fraction, number of fuel blocks, and fuel block re-design to optimize core reactivity. A more compact core should be able to achieve flux levels that approach those of the ATR.

The preliminary reactor physics scoping studies here will lead to additional core configurations to evaluate; core configurations that will include optimizations that approach the goals of a test reactor or irradiation facility, in particular maximizing the irradiation flux and cycle length. The following future steps will be implemented to achieve these two primary goals:

- (1) Develop and evaluate potential core configurations in addition to the three configurations considered here for criticality, thermal and fast irradiation flux levels, and power-peaking.
- (2) Three-dimensional core depletion studies utilizing the 1/12 unrodded core models. Cycle lengths will be determined for different core configurations and PFs or U-235 core mass loadings.
- (3) Optimize the fuel block. The FSV fuel block is currently the baseline block design, but changes to the flat-to-flat dimension, number of fuel rods and coolant channels, fuel rod radius, lattice pitch, PF, and enrichment could help optimize core reactivity and provide a more uniform balance to other variables.
- (4) Burnable poisons. The use and placement of burnable poisons in strategic core locations may be necessary to reduce power-peaking in certain fuel rods or block regions to not over-power TRISO fuel particles beyond limits.
- (5) Control rod design. Develop a control rod design and evaluate the effectiveness over multiple cycles.
- (6) Water ingress. Evaluate the core reactivity effect due to the ingress of water in the coolant channels.
- (7) Irradiation facilities. Evaluate irradiation facility designs with (a) high pressure (including supercritical) light water, (b) hot liquid salt fluids (KF-ZrF, LiF-BeF, etc.), (c) supercritical carbon dioxide, and (d) high-temperature helium and helium-argon gases.
- (8) Develop additional MCNP neutron cross section library data at finer temperature increments.

The next effort for the thermal-hydraulics investigations will be to develop models of the 6- and 12-column core configurations. Different axial power shapes will be investigated. As core design parameters become better defined, iterative calculations between the reactor physics (power distribution) and thermal-hydraulics (fuel and moderator temperatures) will be performed to better define the reactor steady

state conditions. Design-basis accident simulations can then be performed. Parametric studies on different conditions in the irradiation facilities (fluids and temperatures) will also be performed.

5. References

- DOE/HTGR-86-024, 1986, *Preliminary Safety Information Document for the Standard MHTGR*, Stone & Webster Engineering Corp., report HTGR-86-024, 1986.
- RELAP5-3D Code Development Team, 2014, *RELAP5-3D Code Manual, Volumes I-V*, INEEL-EXT-98-00834, Revision 4.2, June 2014.
- X-5 Monte Carlo Team, 2003, *MCNP—A General Monte Carlo N-Particle Transport Code, Version 5*, Volume I (LA-UR-03-1987) and Volume II (LA-CP-03-0245), Los Alamos National Laboratory, Los Alamos, New Mexico, April 23, 2003.